Eur. Phys. J. B **2**, 17–30 (1998)

THE EUROPEAN PHYSICAL JOURNAL B

On the phase diagram of the attractive Hubbard model: Crossover and quantum critical phenomena

J.M. Singer[1,a], T. Schneider[1], and M.H. Pedersen[2]

[1] Physik-Institut, Universität Zürich, Winterthurerstrasse 190, 8057 Zürich, Switzerland
[2] Département de Physique Théorique, Université de Genève, 1211 Genève 4, Switzerland

Received: 5 September 1997 / Accepted: 15 October 1997

Abstract. We explore the phase diagram of the attractive Hubbard model from the point of view of phase transition theory. Using the quantum Monte-Carlo technique, the scaling theory of quantum critical phenomena and the mapping to the XY model we investigate the critical properties along the temperature, band filling and coupling strength axes of the phase diagram. Particular emphasis is devoted to the insulator to superconductor and superconductor to normal metal transitions driven by the variation of the coupling strength U. We also discuss the particular similarities between this simple lattice model and the high-T_c cuprates: both systems exhibit a phase transition along a certain critical line as a function of a particular control parameter, which is *e.g.* the strength of the attractive coupling $|U|$ in the case of the Hubbard model and the electron doping in the copper oxide planes for the cuprates; both show a remarkable crossover along this phase transition line with similar consequences. At one end point (overdoped/small-U regime) we find a behavior similar to a conventional BCS-type superconductor, the system undergoes a normal metal to superconductor transition (NS), whereas at the other end (underdoped/large-U limit) a description in terms of Bose-Einstein condensation (BEC) of preformed pairs is more adequate, with a superconductor to insulator critical endpoint (SI). There superconductivity occurs when the phases of the pairs become coherent, not when the pairs are initially formed. In addition to the fixed electron density, interaction driven crossover the Hubbard model undergoes a further $T = 0$ quantum transition from a (super-) conductor to an insulator for $\rho \to 0$.

PACS. 71.10.Fd Lattice Fermion models (Hubbard model, etc.) – 74.25.Dw Superconductivity phase diagrams – 02.70.Lq Monte-Carlo and statistical methods

1 Introduction

Many physical properties of cuprate superconductors depend on hole doping. The generic doping dependence of the transition temperature T_c is schematically depicted in Figure 1. At a certain doping level x_u, the so-called underdoped limit, the materials undergo at $T > 0$ an insulator to anomalous metal transition, and at $T = 0$ an insulator to superconductor transition. As x is increased T_c rises rapidly and attains a maximum at x_m (optimum doping).

This behavior appears to be a generic feature of the cuprate superconductors [1–3]. In some compounds a further increase of the doping level leads to more metallic normal state properties, but T_c now decreases and falls to zero in the overdoped limit x_0. Here, these materials undergo at $T = 0$ a superconductor to normal metal transition.

Although the schematic phase diagram looks quite symmetric, there are fundamental differences between the underdoped and the overdoped regime: For example, the temperature dependence of the static spin susceptibility from NMR Knight shift measurements [4] shows a pronounced bending and decrease far above T_c in the underdoped regime ("spin gap"). Recent spectroscopic experiments established the existence of a pseudogap in the normal state of underdoped cuprates [5,6]. This pseudogap (*i.e.* the suppression of the single particle density of states) opens not at the superconducting transition temperature T_c, but at a much higher temperature, signalling the existence of paired carriers whithout long-range coherence [7,8]. Superconductivity, however, does not form without this long-range coherence among the pairs, which is established at a lower temperature. Indirectly, the gap is also inferred from a variety of other experiments probing the thermodynamics of charge and spin excitations. The contribution of the new experiments was to show that the pseudogap above T_c has essentially the same magnitude and symmetry as in the state below T_c. Further support for this insulator to superconductor to normal metal scenario in the cuprates comes from recent experiments on the low temperature normal state resistivity from Ando *et al.* [9], as well as from evidence of

[a] e-mail: jms@physik.unizh.ch

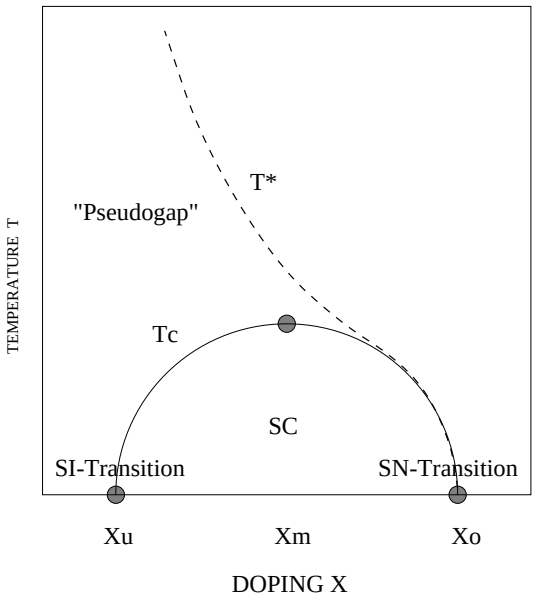

Fig. 1. Schematic temperature-doping phase diagram of the high-T_c cuprates; SC denotes the superconducting state, enclosed by the T_c phase transition line, with x_u, x_m and x_0 marking the underdoped, optimal doped and overdoped case. T^* indicates the temperature, below which the opening of a pseudogap is observed.

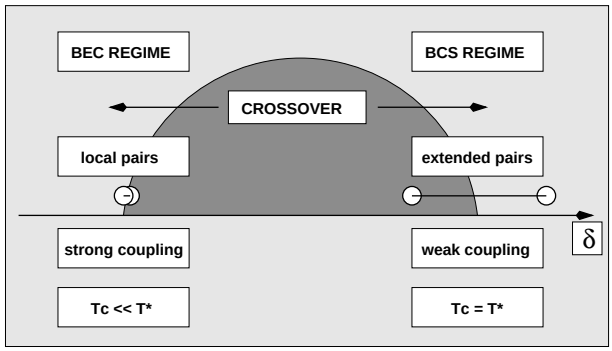

Fig. 2. "Crossover" from a BCS-like endpoint to a BEC endpoint along the superconducting phase transition line. δ symbolizes the control parameter driving the crossover, which is in this diagram associated with the (inverse) coupling strength in case of the attractive Hubbard model and the electronic carrier doping in case of the cuprates.

critical fluctuations above T_c [10]. This normal state pairing scenario is fundamentally different from the BCS model, in which the coherence between pairs is already sufficient for superconductivity when the pairs are formed. But there is an astonishing qualitative similarity to recent discussions of a BCS-type superconductivity to Bose-Einstein-condensation crossover as a function of the coupling strength in the simple 1-band attractive Hubbard model.

It is evident that the attractive onsite density-density interaction term favors double occupancy of sites and hence the formation of pairs. If these pairs of charge $2e$ are mobile, superconductivity will occur below a critical temperature. Because of this conceptual simplicity, the attractive Hubbard model allows an easy investigation of the crossover from low to strong coupling, from extended to local pairs, from BCS-like superconductivity to a Bose-Einstein condensation (BEC) of local pairs, just by tuning the interaction parameter U, which acts as a control parameter for the phase transition line in analogy to the carrier doping in case of the cuprates. The evolution from Cooper-pair superconductivity for small U to local pair superconductivity for large U is smooth. Since both in the small- and large-U limit T_c vanishes, evidently there must be an optimal T_c for an intermediate value of $|U|/t$. In that sense it forms the basic minimal model to give the proper phase transition phenomenology. Nevertheless, we certainly do not propose the negative-U model as a realistic microscopic high-T_c model itself, but use it to deepen our understanding of the phase diagram of high-T_c materials and to explore the effects of pairing fluctuations on various thermodynamic properties (density of states, spin susceptibility *etc.*). Indeed, from the aspect of universality and critical phenomena our analysis strongly reveals close similarities between the overdoped regime in the cuprates and the weak coupling regime of the attractive Hubbard model (both are close to a superconductor—normal metal critical point) on the one side, and the underdoped respectively strong coupling regimes (which are close to a superconductor to insulator critical point) on the other side (see schematic diagrams, Figs. 1 and 2).

2 The attractive Hubbard model

We consider the 2D attractive Hubbard model ("negative-U model") on a square lattice:

$$\mathcal{H} = -t \sum_{\langle ij\rangle\sigma} (\mathrm{c}^\dagger_{i\sigma}\mathrm{c}_{j\sigma} + h.c.) - U \sum_i n_{i\uparrow}n_{i\downarrow} - \mu \sum_{i\sigma} n_{i\sigma}, \tag{2.1}$$

where $\mathrm{c}^\dagger_{i\sigma}$ ($\mathrm{c}_{i\sigma}$) denote fermionic creation (annihilation) operators at site i with spin σ, and t is the kinetic term between two neighboring sites, which serves as an energy unit throughout the paper. The limit $\langle ij\rangle$ restricts the sum to next-neighbors, U denotes the interaction ("coupling"), which is chosen to be attractive, and μ is the chemical potential.

In the free case ($U/t = 0$) we have the well-known dispersion relation for the D-dimensional system,

$$\epsilon(k) = -2t \sum_{\alpha=1}^{D} \cos(k_\alpha) - \mu. \tag{2.2}$$

With the exception of the critical endpoints and $\rho = 0.5$ (ρ is the density of electrons per site and per spin, *i.e.* $\rho = 1$ corresponds to the fully occupied lattice with 2 electrons of opposite spin at each site), the phase transition line is supposed to be a line of D-dim. XY critical points, while the special point $\rho = 0.5$ corresponds to a D-dim.

XYZ critical point. For this reason the transition temperature vanishes in 2D at $\rho = 0.5$ (halffilling); one finds a coexistence of superconducting and long-range charge-density correlations, which, in 2D, drive the effective KT transition temperature to zero, $T_{KT}^{2D}(\rho = 0.5) = 0$, accounting for another critical point $\rho_{\rm c}^{2D} = 0.5$. At zero temperature $T = 0$ there are two critical endpoints, namely $\rho_{\rm c} = 0$ and $\rho_{\rm c} = 1$, where the model undergoes an insulator to superconductor transition.

In addition to the density-driven transitions there are also interaction driven transitions, which we want to focus on in the further context of this report: As a function of coupling strength U and fixed ρ there is a phase transition line with critical endpoints $U = 0$ and $U = \infty$. At $T = 0$ a normal metal to superconductor transition occurs at $U = 0$, while at $U = \infty$ there is a superconductor-localization (insulator) transition. In the strong coupling regime this model can be mapped onto hard core bosons on a lattice, in which Cooper pairs are treated as conserved particles obeying Bose statistics.

3 Methods

3.1 Quantum Monte-Carlo and Hartree-Fock

Our central numerical technique is the temperature-dependent formulation of a Quantum Monte-Carlo (QMC) algorithm in the grandcanonical ensemble, which is largely based on the work of Hirsch, supplemented by the Maximum Entropy method for analytic continuation to extract spectral properties [12,13]. For technical detail we refer to references [11,14].

Additionally we supplement our QMC data with discrete lattice Hartree-Fock calculations (BCS-type) using the standard gap equation for s-wave superconductors ($\Delta(k) = \Delta$) with local interaction $V(k) = U$,

$$\frac{1}{U} = \sum_k \frac{1}{2E(k)} \tanh\left(\frac{\beta E(k)}{2}\right) \tag{3.1}$$

and

$$2\rho - 1 = -\sum_k \frac{\epsilon(k)}{E(k)} \tanh\left(\frac{\beta E(k)}{2}\right) \tag{3.2}$$

with the extended interacting dispersion

$$E(k) = \sqrt{\epsilon(k)^2 + \Delta^2}, \tag{3.3}$$

respectively in terms of the density of states

$$\frac{1}{U} = 2\int_{\omega_B}^{\omega_{\rm T}} \frac{N(\omega){\rm d}\omega}{\sqrt{\omega^2 + \Delta^2}}\,. \tag{3.4}$$

$\epsilon(k)$ is the dispersion in the noninteracting case (Eq. (2.2)), $\beta = 1/T$ the inverse temperature, Δ the gap, $\bar{\mu} = \mu - \rho U$ the chemical potential including a Hartree shift, and U the strength of the attractive interaction; $\omega_{\rm T}$, $\omega_{\rm B}$ are the respective top and bottom band edges of the density of states $N(\omega)$. Because Δ vanishes at and above $T_{\rm c}$, the gap equation also fixes the transition temperature.

Using a Bogoliubov-Hartree-Fock approximation Denteneer *et al.* [15] derived the following explicit formula for the helicity modulus $Y_{\rm s}$ of the 2D attractive Hubbard model

$$\begin{aligned}\Upsilon_{\rm s}^{\rm HF} = &-\frac{t}{N} \\ &\times \sum_k \Big(\frac{\epsilon(k)}{2E(k)} \cos(k_x) \tanh(\beta E(k)/2) \\ &+ \frac{t\beta \sin^2(k)}{2\cosh^2(\beta E(k)/2)} \Big).\end{aligned} \tag{3.5}$$

The expression reduces in the groundstate ($\beta \to \infty$) to

$$\Upsilon_{\rm s}^{\rm HF}(T=0) = -\frac{t}{N}\sum_k \frac{\epsilon(k)\cos(k_x)}{2E(k)} \equiv \frac{1}{8}\int_{\omega_{\rm B}}^{\omega_{\rm T}} \frac{N(\omega)\omega^2 {\rm d}\omega}{\sqrt{\omega^2+\Delta^2}}. \tag{3.6}$$

Comparisons with quantum Monte-Carlo data show remarkably good qualitative and even quantitative agreement with this expression [15–17].

In the strong coupling limit ($\delta(= 1/U) \to 0$), noting that $T_{\rm c} \propto t^2/U$, it is readily seen that $\Upsilon_{\rm s}(T)$ becomes temperature independent, approaching

$$\lim_{U\to\infty} \Upsilon_{\rm s}^{\rm HF}(T) = \Upsilon_{\rm s}^{\rm HF}(T=0) \approx \frac{1}{2DU}\int_{\omega_{\rm B}}^{\omega_{\rm T}} {\rm d}\omega N(\omega)\omega^2. \tag{3.7}$$

In $D = 2$ dimensions this reduces to

$$\Upsilon_{\rm s}(T=0, U\to\infty) = \frac{t^2}{U}\,. \tag{3.8}$$

Next we consider the weak coupling regime, $U \to 0$, where the superconductor to normal metal transition occurs. The helicity modulus tends for $U \to 0+$ to a finite value,

$$\Upsilon_{\rm s}(T=0, U\to 0+) > 0, \tag{3.9}$$

while it is clearly strictly zero for $U = 0$, thus leading to a discontinuous behaviour at the normal metal to superconductor critical point.

In this regime the transition temperature becomes very small, the helicity modulus (Eq. (3.5)) may be written as

$$\begin{aligned}\Upsilon_{\rm s}^{\rm HF}(T) = &\Upsilon_{\rm s}^{\rm HF}(T=0) \\ &- \sum_k \left(2t^2 \sin^2(k_x) \left(-\frac{\partial f(\beta E(k)/2)}{\partial E(k)} \right) \right),\end{aligned} \tag{3.10}$$

$$f(x) = (\exp(x) + 1)^{-1}, \tag{3.11}$$

where $\Upsilon_{\rm s}^{\rm HF}(T=0)$ is given by the above expression. Close to $T_{\rm c}^{\rm HF}$ equation (3.5) reduces to

$$\frac{\Upsilon_{\rm s}^{\rm HF}(T)}{\Upsilon_{\rm s}^{\rm HF}(T=0)} \approx 2\left(1 - \frac{T}{T_{\rm c}^{\rm HF}}\right). \tag{3.12}$$

3.2 Scaling theory of quantum critical phenomena

The scaling theory of quantum transitions (see *e.g.* Refs. [18–21]) is based on the central assumption that a single characteristic length scale ξ exists near the transition, which diverges by approaching the critical point. For a phase transition driven by the temperature, $T - T_c$, the difference from the critical temperature, measures the distance from the critical point. At a transition like metal-insulator, which is basically a quantum phase transition at $T = 0$, the phase transition is controlled by quantum fluctuations through parameters such as the band width or the chemical potential rather than the temperature, *i.e.*, in contrast to finite temperature, where static critical phenomena can be discussed with no regard to the systems dynamics, the fluctuations at zero temperature are purely quantum mechanical, so that static and dynamic quantities are linked. We assume the existence of a field, controlling the phase transition, which we denote with the dimensionless quantity δ (control parameter). For example we assume at a MI-transition for the metallic and the insulating phases $\delta > 0$ and $\delta < 0$, respectively, and $\delta = 0$ gives the critical point.
(a) The correlation length exponent $\bar{\nu}$ determines how ξ diverges as $\delta \to 0$ ("spatial correlation length")

$$\xi = \xi_0^{\pm} |\delta|^{-\bar{\nu}} \tag{3.13}$$

and (b) the temporal correlation length is given *via*

$$\xi_\tau = \xi_{\tau,0}^{\pm} |\delta|^{-\nu_\tau}. \tag{3.14}$$

A characteristic frequency is determined from this dynamics

$$\Omega \propto \xi^{-z} \tag{3.15}$$

with the dynamical critical exponent

$$z = \frac{\nu_\tau}{\bar{\nu}}\,. \tag{3.16}$$

At positive temperatures the imaginary temporal extent, $0 \le \tau \le \beta$ of the system is finite. Thus, ξ_τ does not diverge and the quantum dynamics do not affect the static critical behavior; only at $T = 0$, ξ_τ may diverge.

When it does, the classical hyperscaling argument must be modified, which leads the free energy singular part f_s to the form

$$f_s \propto \xi^{-d} \xi_\tau^{-1} \propto |\delta|^{2-\bar{\alpha}}. \tag{3.17}$$

Using the above definitions this yields the generalized hyperscaling relation

$$2 - \bar{\alpha} = \bar{\nu}(D + z), \tag{3.18}$$

with D being the dimension of the system. The corresponding universal amplitude relation is

$$\mathcal{R}_\tau^{\pm} = \xi_{\tau 0}^{\pm} \xi_0^D \mathcal{A}^{\pm}, \tag{3.19}$$

at $T \to 0$ we define α and $\mathcal{A}^{\pm}$ *via*

$$\kappa := -\frac{\partial^2 f_s}{\partial \delta^2} \approx \frac{\mathcal{A}^{\pm}}{\alpha} |\delta|^{-\alpha}. \tag{3.20}$$

One generic choice for δ is the chemical potential μ; in this case κ corresponds to the compressibility, and the band filling is given *via* the first derivative of f_s. Above some critical dimension $D = D_c$ hyperscaling is violated.

The occurrence of superfluidity is conveniently described in terms of the free energy density in the presence of an imposed order-parameter twist with wave vector k_0, from which one derives the helicity modulus

$$\Upsilon_s(\delta) = \lim_{k_0 \to 0} \frac{\partial^2 f_s}{\partial k_0^2} \tag{3.21}$$

(see above, Eq. (3.5)), with a related diverging length in the ordered phase as

$$\xi^{\Upsilon} = (\xi_\tau(\delta)\Upsilon(\delta))^{1/(2-D)}. \tag{3.22}$$

Therefore according to the scaling theory of phase transitions T_c and the helicity modulus vanish as

$$T_c = \mathcal{E} |\delta|^{z\bar{\nu}} \tag{3.23}$$

$$\Upsilon_s = \lim_{k_0 \to 0} \frac{\partial^2 f_s}{\partial k_0^2} = F |\delta|^{2-\bar{\alpha}-2\bar{\nu}} = F |\delta|^{\bar{\nu}(D+z-2)}. \tag{3.24}$$

It is important to recognize that relation equation (3.24) requires the validity of hyperscaling, while equation (3.23) follows directly from finite size scaling in the time direction.
In $D = 2$ the ratio

$$\lim_{\delta \to 0} \frac{\Upsilon_s(\delta)}{T_c(\delta)} = \frac{F}{\mathcal{E}} = Q_0 \tag{3.25}$$

is then an universal number, with a characteristic value within a particular universality class. It undergoes in the strong coupling limit – the regime, where the attractive Hubbard model corresponds to hard core bosons on a lattice – at $T = 0$ for $U \to \infty$ a superfluid-insulator transition, with $z\bar{\nu} = 1$, $\bar{\nu} = \frac{1}{2}$, $\alpha = 0$, where

$$\delta = t/U. \tag{3.26}$$

Moreover, it follows that

$$\Upsilon_s(\delta) \propto T_c(\delta)^{\frac{D+z-2}{z}}, \tag{3.27}$$

with a nonuniversal proportionality factor in $D > 2$.

3.3 Approximate treatment of the phase transition line

An approximate treatment of the phase transition line is readily obtained by mapping the finite temperature behavior of the Hubbard Hamiltonian onto the classical XY-model. This mapping assumes that the order parameter

is a complex scalar, corresponding to a spin vector with $n = 2$ components. This mapping is not applicable for the particular case $\rho = 0.5$, where the order parameter, as mentioned above, adopts $n = 3$ components.
A Ginzburg-Landau functional for this model has then the form [22]

$$\mathcal{F} = \sum_l \Big(a(|T|)|\Delta_l|^2 + b(T)|\Delta_l|^4 + c(T) \sum_\nu |\Delta_l - \Delta_{l+\nu}|^2 \Big). \tag{3.28}$$

l denotes the lattice sites and ν denotes the nearest neighbors on a hypercubic lattice. Neglecting amplitude fluctuations in the order parameter,

$$\Delta_l = |\Delta_l| \exp(i\phi_l) \equiv \Delta_0 \exp(i\phi_l),$$

the functional $\mathcal{F}$ reduces to

$$\mathcal{F} = N \left(a(|T|)\Delta_0^2 + b(T)\Delta_0^4 \right) + J(T) \times \sum_{l,\nu} (1 - \cos(\phi_l - \phi_{l+\delta})), \tag{3.29}$$

$$J(T) = 2\Delta_0^2 c(T), \tag{3.30}$$

corresponding to the classical D-dimensional XY-model with nearest neighbor coupling $J(T)$:

$$\mathcal{H}_{XY} = -J(T) \sum_{l,\nu} \cos(\phi_l - \phi_{l+\delta}) \tag{3.31}$$

with the transition temperature (into a ferromagnetically ordered state corresponding to superconducting order *via* the above shown identification (3.30))

$$T_\mathrm{c} = QJ(T_\mathrm{c}), \tag{3.32}$$

where Q depends on dimensionality. Recent Monte-Carlo estimates [23,24] are for

$$\text{2D}: \quad Q \approx 0.898, \tag{3.33a}$$
$$\text{3D}: \quad Q \approx 2.202. \tag{3.33b}$$

Neglecting topological excitations, Hamiltonian (3.31) reduces to

$$\mathcal{H}_{XY} = -\frac{J(T)}{2} \int \mathrm{d}^D r (\nabla\phi)^2. \tag{3.34}$$

The helicity modulus is then simply

$$\Upsilon_\mathrm{s}(T) = J(T) \tag{3.35}$$

and given by the previously shown Bogoliubov-Hartree-Fock expression (3.5) for $\Upsilon_\mathrm{s}^\mathrm{HF}$.
In combining the equations (3.5), (3.32) and (3.35) we find for the D-dimensional Hubbard model the equation

$$T_\mathrm{c} \approx Q\Upsilon_\mathrm{s}^\mathrm{HF}(T_\mathrm{c}). \tag{3.36}$$

Its solution provides estimates for the phase transition line. The transition temperature is then defined as the temperature where the Hartree-Fock expression for the helicity modulus (3.5) coincides with relation (3.36). The resulting critical temperature T_c is smaller than the Hartree-Fock estimate T_c^HF, the reduction vanishes for $|U| \to 0$. In the weak coupling regime, $U \to 0$, equations (3.12) and (3.36) yield

$$T_\mathrm{c} \approx \frac{2Q\Upsilon_\mathrm{s}^\mathrm{HF}(T=0)}{1 + \frac{2Q\Upsilon_\mathrm{s}^\mathrm{HF}(T=0)}{T_\mathrm{c}^\mathrm{HF}}} \underset{U\to 0}{\longrightarrow} T_\mathrm{c}^\mathrm{HF}. \tag{3.37}$$

Thus, in the weak coupling limit we recover asymptotically the Hartree-Fock transition temperature given by the gap equation.
For $D = 2$ one obtains in the strong coupling limit $U \to \infty$ with equations (3.32) and (3.36)

$$T_\mathrm{c}(U \to \infty) = Q\Upsilon_\mathrm{s}^\mathrm{HF}(U \to \infty) \approx 0.898 \frac{t^2}{U}. \tag{3.38}$$

We note that this relation also follows from the scaling theory as described in Section 3.2, stating that in $D = 2$ and close to the superconductor to insulator transition the ratio $Q_0 \approx 1/0.898 = 1.114$ (Eq. (3.25)) becomes universal. From degenerate perturbation theory and the fact that the insulator is not compressible the relevant critical exponents can be derived explicitly. It then follows that the superconductor to insulator transition occurring at $U \to \infty$, *i.e.* control parameter $\delta \to 0$, is in the universality class of the generic superfluid to insulator transition. We have seen that equation (3.36) correctly reproduces in both cases, the strong and the weak coupling limit, the essential asymptotic behavior. Therefore it is expected to provide a rather reasonable description of the phase transition line.

3.3.1 Ideal Bose gas

As a first example we consider the onset of superfluidity in the ideal Bose gas; for $D = 3$ dimensions we find

$$z\bar{\nu} = \frac{2}{3}, \quad z = 2, \quad \bar{\nu} = \frac{1}{3}, \tag{3.39a}$$

and more generally for $D > 2$:

$$z\bar{\nu} = \frac{2}{D}, \quad z = 2, \quad \bar{\nu} = \frac{1}{D}\,. \tag{3.39b}$$

At finite temperatures the corresponding exponents adopt the values

$$\nu = \frac{1}{D-2}, \quad \alpha = \frac{D-4}{D-2}, \tag{3.40a}$$

$$\gamma = 2\nu = \frac{2}{D-2}, \quad \eta = 0, \quad 2 < D \leq 4. \tag{3.40b}$$

Thus, the critical exponents for the quantum transition at the onset of superfluidity (OS) in an ideal Bose gas are simply the classical ones in $D+2 = D+z$ dimensions, *i.e.*

$$\bar{\nu} = \nu(D+2) = \nu(D+z). \tag{3.41}$$

3.3.2 Non-interacting fermions: Density-driven metal to insulator transition

Next we want to discuss non-interacting fermions ($U/t = 0$) with an energy given by equation (2.2). At $T = 0$ a metal to insulator transition occurs when the chemical potential μ approaches the bottom of the band,

$$\mu \to \mu_{\mathrm{B}} \equiv -2Dt. \tag{3.42}$$

In this limit we can derive the following critical exponents:

$$z = 2, \quad \eta = 0, \tag{3.43}$$

$$\bar{\nu} = \frac{1}{2}, \quad \bar{\alpha} = \frac{D-2}{2}\,. \tag{3.44}$$

The upper critical dimension is $D_{\mathrm{c}} = 2$, following from the hyper-universal exponent relation.
This leads us finally to the relation between the chemical potential μ and the bandfilling ρ

$$\rho \propto (\mu - \mu_{\mathrm{B}})^{1/2} \quad : D = 1 \tag{3.45a}$$
$$\rho \propto (\mu - \mu_{\mathrm{B}}) \quad : D = 2 \tag{3.45b}$$
$$\rho \propto (\mu - \mu_{\mathrm{B}})^{3/2} \quad : D = 3. \tag{3.45c}$$

3.3.3 Interaction driven transitions

Collecting previous remarks we find:
(1) For fixed band filling the model undergoes at $T = 0$ and $U \to 0$ a superconductor to normal metal transition; in the weak coupling limit the Hartree-Fock or BCS approximation is expected to become exact. Using the HF expressions we obtain the following critical exponents:

$$z\bar{\nu} = \frac{1}{2}, \quad \bar{\nu} = \frac{1}{2}, \quad z = 1, \quad \bar{\alpha} = 0. \tag{3.46}$$

(2) The strong coupling treatment provides for the exponents

$$z\bar{\nu} = 1, \quad \bar{\nu} = \frac{1}{2}, \quad z = 2, \quad \bar{\alpha} = 0. \tag{3.47}$$

4 Results: Phase diagram

In general the phase diagram of the attractive Hubbard model is three-dimensional, depending on the coupling strength $|U|$, the fermion (electron) density ρ and the temperature T.

First we want to present quantum Monte-Carlo results for a U-T-phase diagram of the attractive Hubbard model. We examined the 2D attractive model at an electron density $\rho = 0.4$ per spin and lattice site, which approximately corresponds to a maximum in $T_{\mathrm{c}}(\rho)$ for fixed U. In $D = 2$ at halffilling, T_{c} is zero, due to the coexistence of superconductivity and CDW long-range order. There the system has Heisenberg symmetry, which does not allow for the 2D KT-phase and therefore gives $T_{\mathrm{c}} = 0$. Nevertheless a small deviation from halffilling destroys the Heisenberg symmetry and results in a finite T_{c}, with a maximum around $\rho = 0.4$. Our own findings are in good agreement with reference [25].

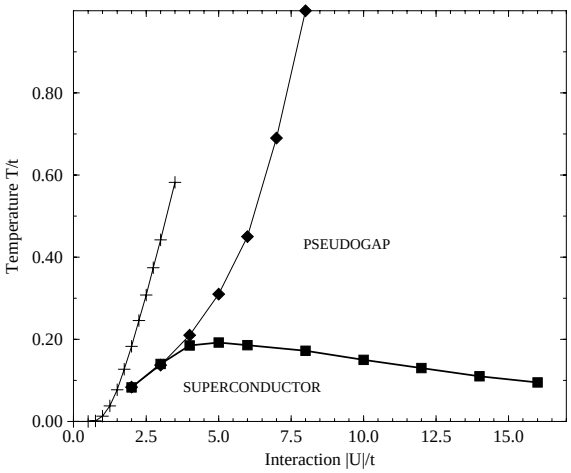

Fig. 3. Temperature-interaction phase diagram of the attractive 2D Hubbard model, electron density per spin is $\rho = 0.4$. The filled square symbols represent the QMC phase transition line (T_{c}) into the superconducting state ("superconductor"), measured *via* ODLRO in the s-symmetric pair correlation function (unscaled). The rhombic symbols denote the temperature T^*, below which a gap ("pseudogap") in the single particle density of states is detected, and the line with cross symbols shows the Hartree-Fock phase-transition line from normal to superconducting state.

Figure 3 shows our QMC-results: we clearly find evidence for a phase coherent superconducting state below a critical condensation temperature T_{c} (or rather T_{KT} in a strict sense), in agreement with reference [25]; it is detected as the inflection point in the long-range plateau value of the s-wave pair correlations [11] as a function of temperature,

$$\chi_{\mathrm{s}}(l) = \langle \Delta^\dagger(0)\Delta(l) + \Delta(0)\Delta^\dagger(l) \rangle, \tag{4.1}$$

where

$$\Delta^\dagger(l) = \mathrm{c}_l^\dagger \mathrm{c}_l^\dagger. \tag{4.2}$$

The presented data are obtained for one particular finite lattice (10×10 sites); they are not size scaled and provide therefore only an upper bound. We augment the QMC data in Figure 3 with a curve showing the estimates of the HF theory for the transition temperature T_{c}, which gives a monotonically increasing transition temperature with increasing coupling strength U. This is in sharp contrast to the QMC data, which show a saturation around $U/t = 5$ and even a suppression for large coupling strengths, indicating a crossover from mean field-like behavior, which describes the small-U region very well, to a local pair

superconductivity (for which $T_c \to 0$ for $|U|/t \to \infty$). The strong coupling behavior is rather well described by a t/U-proportionality.

In addition we plot in Figure 3 T^*, extracted from density of states data $N(\omega = 0, T)$: The temperature dependence of the density of states at zero frequency shows a suppression for decreasing T due to pairing fluctuations ("pseudogap"). We defined T^* equivalently to T_c as the inflection point in $N(\omega = 0, T)$. This is strictly speaking an underestimation, since the gap itself certainly starts to occur earlier, but a numerical detection of a 'first occurrence' from a discrete set of data points is rather difficult and unreliable. Furthermore, we want to remind that the spectral QMC data are obtained *via* an analytical continuation with the maximum entropy method [12,13], giving rise to an additional degree of uncertainty in the estimation of very tiny features. The pseudogap becomes only detectable if it has already a rather large size. Usually one associates the *first* appearance of a pseudogap dip in the DOS with T^*, thus finding even higher values for T^* (which indeed brings T^* even closer to the mean field prediction for T_c).

The three temperature regimes $T \gg T^*$, $T^* > T > T_c$ and $T_c \geq T$ can also be clearly detected in the shape of the bandstructure, Figure 5. The bandstructure is obtained by plotting the QMC momentum resolved spectral density $A(k, \omega)$ *vs.* k, ω (see Ref. [11], note that $N(\omega) = \sum_k A(k, \omega)$). The high temperature regime $T \gg T^*$ has predominantly single-band character; this single band splits with decreasing temperature well above T_c into two distinct bands. These bands change their shape to a system of bands similar to the prediction of *e.g.* a BCS theory of superconductivity, when the system undergoes its phase transition into a coherent state at T_c. It should be noted that the change of the band structure from the normal state pseudogap regime to the superconducting regime causes a distinct change of the density of states: In the superconducting regime we find extended 'flat' band regions (visible around $k = (\pi, 0)$ in Fig. 5c), which produce a density of states peak at the gap edges. These gap-edge peaks allow a distinction between the normal state and superconducting state gap, although both have the same absolute width. Such a feature is also experimentally found in ARPES experiments on underdoped cuprates below the transition from the pseudogap to the phase coherent regime ('coherent particle peak' [26]). The peak itself has previously been observed a rather long time ago by Baer *et al.* [27] in a photoemission study of the BSCCO compounds. Our results show that the superconducting transition in the Hubbard model is clearly associated with a change in the shape of the band structure and thus the density of states. For details we refer to reference [28].

The occurrence of a gap in the single particle density of states is connected with anomalies in several response quantities, like *e.g.* a suppression of the static spin susceptibility $\chi_s(k = 0, \omega = 0, T)$, Figure 6, above T_c at the same temperature T^*, indicating a spin-singlet formation. T^* goes to higher temperatures for increasing $|U|$. A full

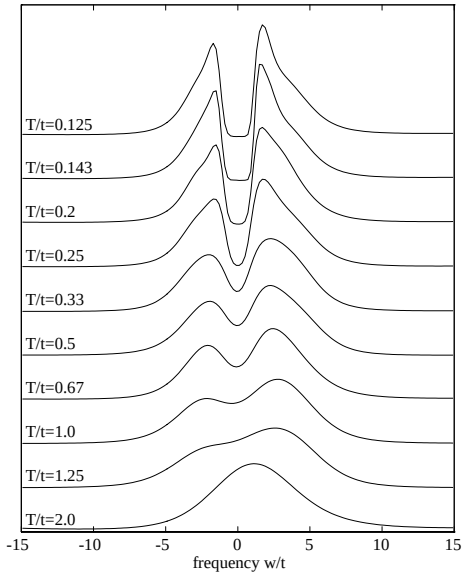

Fig. 4. Attractive Hubbard model, QMC, single particle density of states $N(\omega, T)$ for a series of temperatures, obtained with Maximum Entropy analytic continuation. The superconducting transition temperature T_c measured by the appearance of superconducting long-range correlations is below $T/t = 0.2$, whereas the gap in the DOS as an indicator for pair formation already appears at much higher temperatures. T^* (Fig. 3) is measured as the inflection point in $N(0, T)$. $\rho = 0.4$, $U/t = -6.0$

description of the crossover from weak to strong coupling superconductivity can be found in reference [11] and citations therein. We attribute T^* to a pair formation already in the normal state, it is easy to see in Figures 4-6 that the gap in the DOS appears at temperatures far above the critical temperature T_c already for intermediate coupling strength.

Up to now we have a phase transition line for fixed ρ and variation of the control parameter coupling $|U|/t$; this gives us for $T = 0$ a transition from a normal metal at $U = 0$ to a superconductor for finite coupling $|U| > 0$ to an insulator for $U \to \infty$. The weak coupling regime is rather nicely described by a Hartree-Fock approach, as expected, whereas the strong coupling regime shows rather anomalous normal state properties; in particular we want to emphasize the appearance of a gap in the normal state.

We also want to investigate the phase diagram in the temperature-filling hyperplane: $T_c(\rho)$. Figure 7 shows QMC as well as HF data for the filling dependence of T_c: The region around halffilling ($\rho = 0.5$) is rather well described by a Gaussian-like dependency of T_c on ρ. This is true for the QMC as well as the HF data. Nevertheless, this does not account for the earlier mentioned fact that $T_c(\rho = 0.5) = 0$ due to a coexistence of long-range superconducting (SC) and charge density wave (CDW) correlations. The HF approach does not "see" the CDW correlations, whereas the T_c in case of the presented QMC data has been calculated only from pair correlation functions, the CDW correlations are neglected. Clearly,

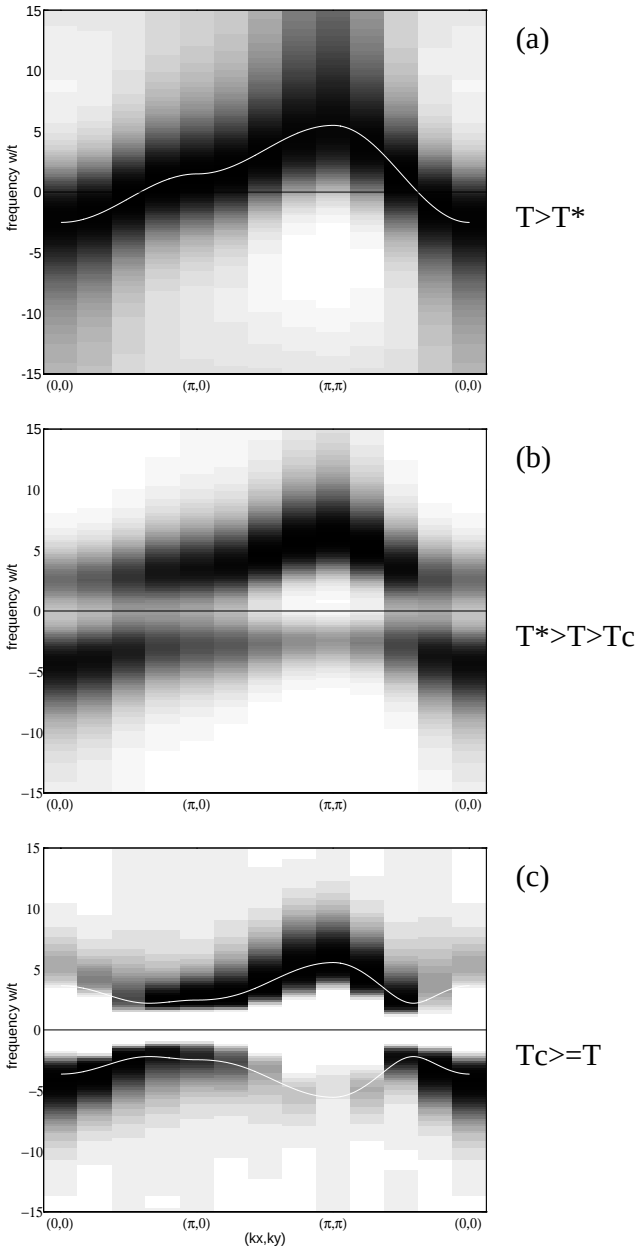

Fig. 5. Attractive Hubbard model, temperature dependence of the bandstructure. The figure shows the spectral weight $A(k,\omega)$ obtained from QMC calculations in a gray shade coding, dark regions mark large values. The data are shown as a function of frequency ω ($\omega = 0$ corresponds to the chemical potential) and momentum vector $\mathbf{k}$ along the usual triangle $(0,0) \rightarrow (\pi,0) \rightarrow (\pi,\pi) \rightarrow (0,0)$. 8×8-system, $U/t = -8.0$, $\rho = 0.4$. The upper picture (a) is taken at very large temperature $T > T^*$, the white line sketches a simple $U/t = 0$ single free band, (b) results from a measurement in the pseudogap regime $T^* > T > T_c$, where the single band splits into two bands, a single particle band and a pair band, and (c) is taken below the transition temperature T_c; the white lines in the lower picture are the HF prediction for the band structure below T_c fitted to the actual gap size.

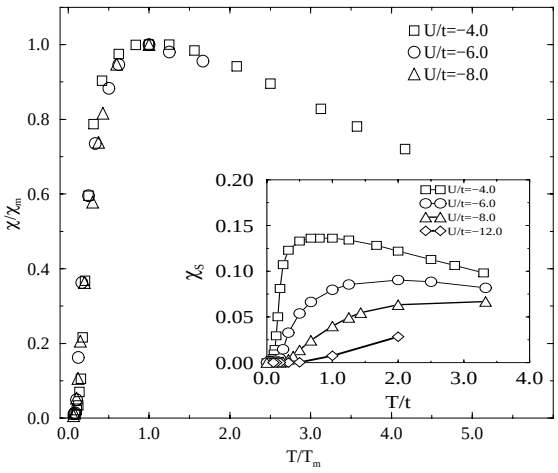

Fig. 6. Attractive Hubbard model, normalized static spin susceptibility χ/χ_m *vs.* normalized temperature T/T_m, QMC data, $\rho = 0.4$, $U/t = -4.0$ (□), $U/t = -6.0$ (◯) and $U/t = -8.0$ (△). T_m denotes the temperature, where χ exhibits its maximum, χ_m is the corresponding value at T_m. Inset: Temperature dependence of the susceptibility $\chi_s(T)$; the down-bending as an indicator for spin-singlet (*i.e.* pair) formation and therefore T^* shifts to higher temperatures for increasing U.

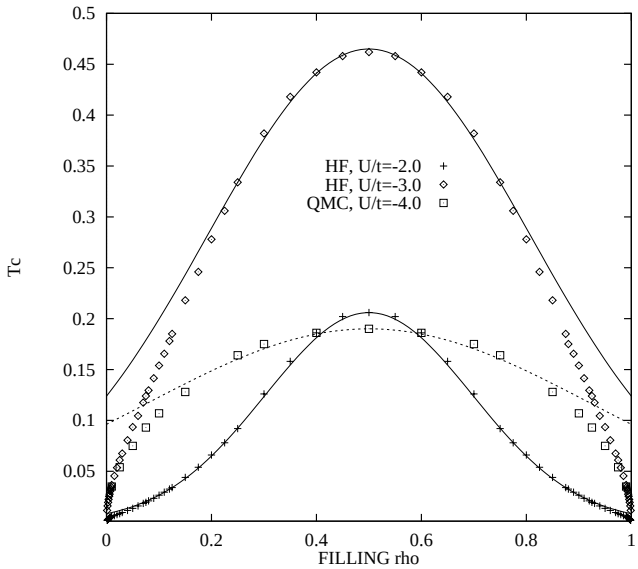

Fig. 7. Critical temperature as function of bandfilling $T_c^{HF,QMC}(\rho)$, Hartree-Fock and QMC data (□). Linear plot, the curves are Gaussians ($b\exp(-(a(\rho-0.5)^2))$) fitting the behavior of the T_c-data for bandfillings around halffilling (HF, $U/t = -2.0$, +; HF, $U/t = -3.0$, (◇); QMC, $U/t = -4.0$, (□). In a rigorous treatment, however, T_c vanishes in 2D for $\rho \rightarrow 0.5$, as explained in the text.

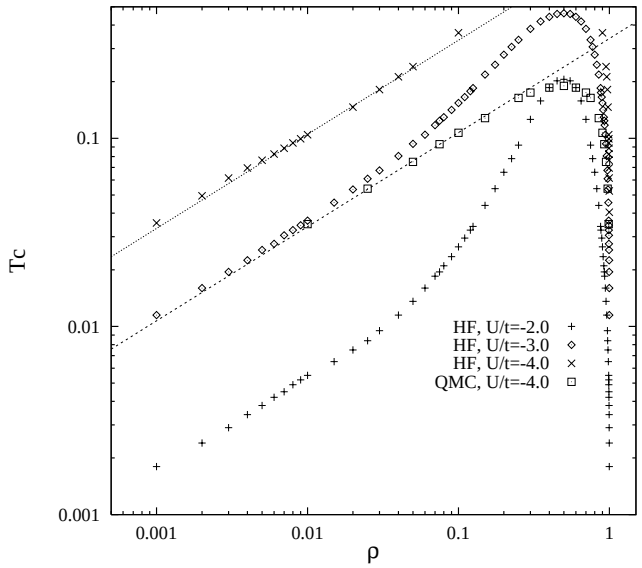

Fig. 8. HF critical temperature as a function of bandfilling, $T_c^{\mathrm{HF}}(\rho)$. $U/t = -2.0(+), -3.0(\diamond), -4.0(\times)$, log-log plot; the behavior in the low density limit $\rho \to 0$ approaches asymptotically a linear curve (solid and dashed curve for different coupling values), corresponding to a power law dependency with exponent 0.5 (square root). QMC data ($U/t = -4.0$, ($\Box$)) are also included, they nicely fit the low density square root behavior ($a \times \rho^{0.5}$, with $a = 0.34$, dashed curve) for a rather extended range almost up to quarter filling.

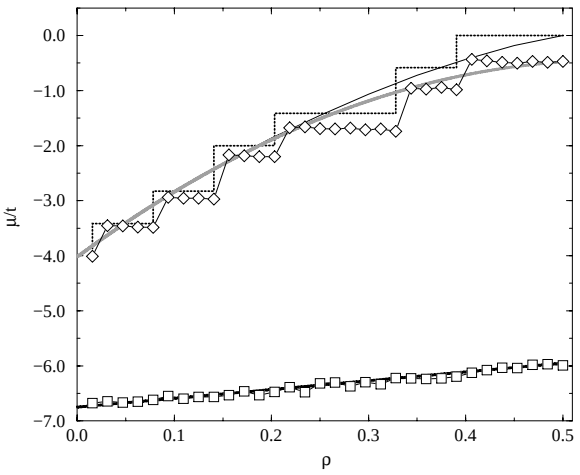

Fig. 9. Chemical potential μ as a function of the filling ρ, ground state ($T = 0$) QMC data, $U/t = -1.0$ ($\diamond$), weak coupling) and $U/t = -12.0$ ($\Box$), strong coupling). The data nicely fit to a parabolic curve ($\mu \propto \rho^2$) in the weak coupling limit (solid grey line) and to a linear curve ($\mu \propto \rho$) in the strong coupling regime (thick black solid line). The steps in the QMC curve results from a finite energy level spacing due to a finite lattice (an appropriate $U = 0$ chemical potential for a 8×8 lattice is included with the dotted curve), which is smeared out in the strong coupling case because of a sufficient line broadening. We include the infinite lattice size HF prediction for $\mu(\rho)$ (thin black solid line) for comparison; it shows no charge gap at halffilling.

the exact QMC data cause a 'renormalization' of the HF data, accounting for the well-known effect of an overestimation of critical temperatures in the framework of mean-field theories.

In the low density limit, $\rho \to 0$, $T_c(\rho)$ undergoes a crossover into a power-law dependency with exponent 0.5 (square-root), which is again found for HF as well as QMC data. This crossover can be nicely seen in the double-logarithmic plot of Figure 8; it shifts for increasing coupling strength to higher densities. $\rho \to 0$ is a trivial normal metal resp. superconductor to insulator transition.

Invoking again the quantum scaling approach one expects $T_c \propto \rho^{z\bar{\nu}}$, so that $z\bar{\nu} = 1/2$. This particular value can be understood in terms of the HF treatment, where $z = 1$, $\bar{\nu} = 1/2$. It is remarkable that the limiting case, where $T_c(\rho)$ adopts a square-root dependency, extends to a very large ρ-region for the QMC data; the dashed line in Figure 8 indicating this power law almost exactly fits the data up to quarter-filling. The 'renormalization' of U can be nicely seen, since the $U/t = -4.0$ QMC curve interpolates between the $U/t = -3.0$ HF curve in the low density limit and the $U/t = -2.0$ HF curve close to halffilling.

Following Furukawa *et al.* [29] we calculated the "average" chemical potential for the canonical ensemble of finite size lattices within the canonical $T = 0$ PQMC formalism, defined by

$$\bar{\mu}(\bar{\rho}) = \frac{E(\rho_1) - E(\rho_2)}{\rho_1 - \rho_2}, \tag{4.3}$$

where $\bar{\rho} = (\rho_1 + \rho_2)/2$, the ρ_i are adjacent integer particle number fillings. In the thermodynamic limit this reduces to

$$\bar{\mu} \to \mu = \frac{\partial E(\rho)}{\partial \rho}\,. \tag{4.4}$$

The results for $\mu(\rho, U)$ are shown in Figure 9: In the weak coupling regime away from halffilling the QMC data are nicely fitted by the Hartree-Fock prediction (besides the usual finite size step – "closed shell" – structure, which vanishes for $L \to \infty$, as shown in Figure 9 with the inclusion of a finite lattice free system μ). At halffilling we find a charge gap Δ_c, in agreement with Furukawa [29], which survives in the thermodynamic limit. $\mu(\rho)$ follows a parabola ($\mu \propto \rho^2$) for finite fermionic densities.

In contrast to this the strong coupling regime is fundamentally different: It is no longer in agreement with the mean field prediction – as expected –, there is a large gap at $\rho = 0.5$ (halffilling), and there is a crossover from a quadratic dependency in the weak coupling regime to a strong coupling linear dependency $\mu \propto \rho$. Note, that the closed shell structure vanishes due to the interaction broadening of the finite size energy levels: A free finite system shows discrete δ-peak levels in the density of states, and therefore the chemical potential remains constant as long as one of these shells gets filled. Approximately,

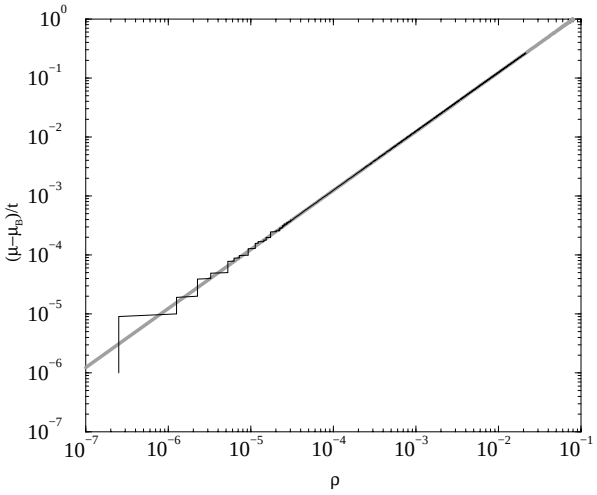

Fig. 10. Chemical potential for the 'free' $U = 0$ system (normal metal) in the limit $\rho \to 0$, $\mu \to \mu_{\rm B}$ ($\mu_{\rm B} = -4t$ in the 2D case). We find a crossover to a strictly linear behavior $\mu \propto \rho$ (well fitted by the relation $\mu = 12.4\rho + \mu_{\rm B}$, grey line) when the system approaches this 'trivial' insulator critical point. Discrete system with 4×10^6 k-space points.

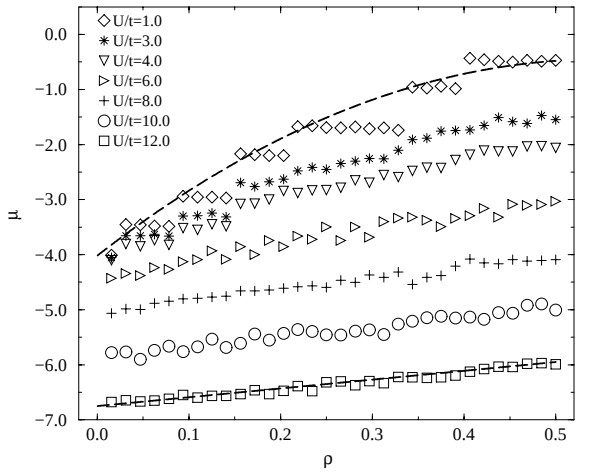

Fig. 11. Chemical potential μ as a function of the filling ρ, ground state ($T = 0$), QMC data, 8×8-lattice. The dashed lines denote the two extremal cases, weak coupling quadratic behavior and strong coupling linear dependency.

this argument is still true in a weakly interacting system. But: This levels become broader with increasing coupling strength until they eventually 'touch' each other and a "quasi-continuous" density of states evolves, giving rise to a continuous $\mu(\rho)$ curve even in a finite system, at least on the level of integer particle increments or decrements. As shown in the ground state QMC-data in Figure 11, this crossover from weak coupling quadratic behavior to strong coupling linear dependence is continuous and takes place in the approximate coupling strength range between $U = 0$ and $U/t = -8$, the latter being the bandwidth of the free system. The charge gap shows in the investigated range a linear dependence $\Delta_{\rm c} \propto U$.

Another crossover takes place in the ($\rho \to 0$)-limit: The system again undergoes a change from the parabolic dependence to a linear one ($\mu \propto \rho$) for all $|U| \geq 0$ and $\rho \to 0$ ("empty lattice insulator"), and thus approaches another insulator critical endpoint (see Fig. 10) when the chemical potential reaches the bottom of the band $\mu_{\rm B}$. If we consider non-interacting fermions ($U = 0$, as shown in Fig. 10) this is

$$\mu \to \mu_{\rm B} \equiv -2Dt \quad (= -4t \text{ in } D = 2 \text{ dimensions}). \quad (4.5)$$

We should mention the fact that $\mu_{\rm B} < -4t$ in the interacting system, $|U| > 0$. The relation between the chemical potential and the band filling is then given by

$$\rho \propto (\mu - \mu_{\rm B}) \quad (4.6)$$

in $D = 2$ dimensions.

Now we want to focus on a more qualitative understanding of the phase diagram, and here in particular of the $T-U$-part (Fig. 3) because of its qualitative similarity to the phase diagram of the high-$T_{\rm c}$ cuprates (Fig. 1). Similar to the crossover found in the cuprates and described *e.g.* in references [1–3] we find a transition from a normal metal to a superconductor to an insulator. In both cases it is driven by a control parameter δ, which is the doped hole concentration x in case of the cuprates and the coupling strength $|U|$ in case of the attractive Hubbard model. The directly corresponding regimes are the weak coupling Hubbard model and the overdoped cuprates, which are both well approximated by a mean field treatment, and the strong coupling Hubbard model and the underdoped cuprates, both deviate strongly from mean field behavior, and both exhibit distinct features like the normal state gap. Therefore we use Sections 3.2 and 3.3 to gain deeper insight: Figure 12 provides a set of ground state helicity modulus data from the Bogoliubov-Hartree Fock approach (Eq. (3.5)): $\Upsilon_{\rm s}(|U|, T = 0)$ for fixed ρ. There are two different limiting cases:

- In the limit of vanishing coupling $U \to 0+$, $\Upsilon_{\rm s}(T = 0)$ tends to a finite value, while it is strictly zero for $U = 0$, therefore leading to a distinct discontinuity (Fig. 12). Any small but finite coupling strength produces a superfluid density, only limited by the electronic carrier density as a reservoir to form pairs. Trivially, $\Upsilon_{\rm s}(T = 0)$ goes to zero for constant U and $\rho \to 0$ (Fig. 13): 'empty lattice insulator'.
- In contrast to the weak coupling regime, $\Upsilon_{\rm s}(T = 0) \to 0$, continuously, for $|U| \to \infty$, and in $D = 2$ one obtains $\Upsilon_{\rm s}(T = 0, |U| \to \infty) \propto 1/U$.

Using the helicity modulus data and equation (3.36) we can approximately describe the phase transition line, as sketched in Section 3.3: The transition temperature is simply defined as the temperature where the Bogoliubov-Hartree Fock expression for the helicity modulus coincides with relation (3.36), see Figure 14. Figure 15 gives

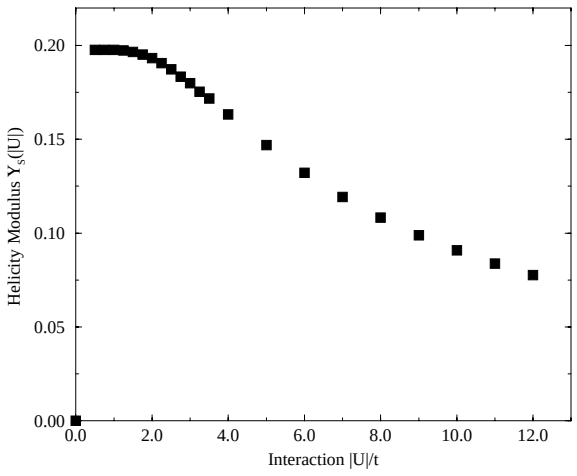

Fig. 12. Helicity modulus Υ_s *versus* $|U|/t$ for $\rho = 0.4$, $d = 2$, $T \to 0$.

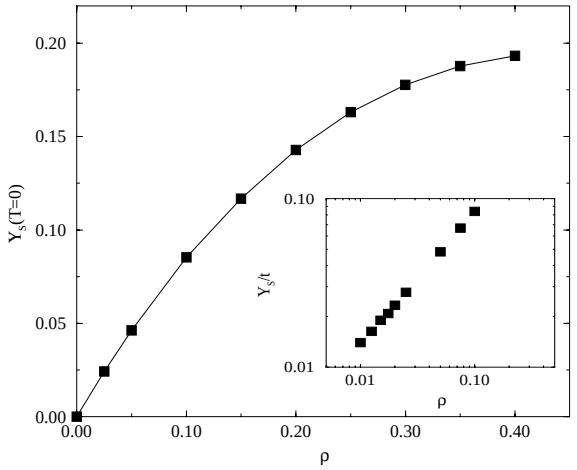

Fig. 13. Helicity modulus $\Upsilon_\mathrm{s}(T = 0)$ *versus* filling ρ, weak-coupling regime, $U/t = -2.0$; inset: logarithmic plot.

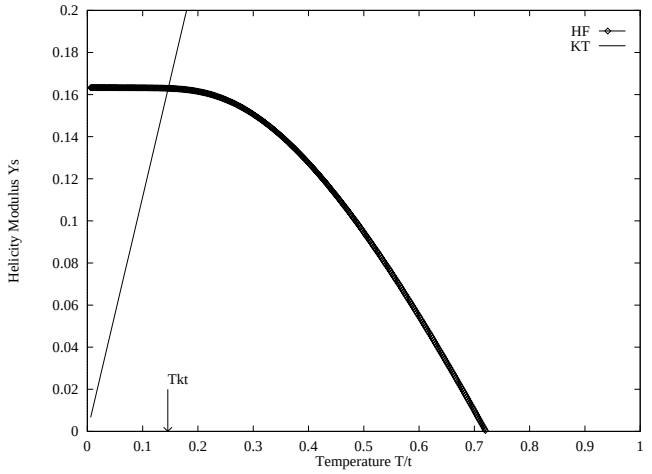

Fig. 14. Estimation of T_c: $\Upsilon_\mathrm{s}^\mathrm{HF}$ *versus* T/t for $\rho = 0.4$, $D = 2$, $U/t = -4.0$, thin line is the KT-relation.

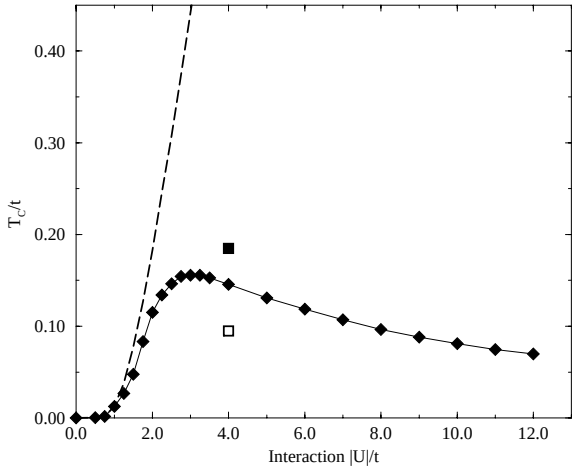

Fig. 15. Phase diagram: T_c *vs.* $|U|$, $\rho = 0.4$, $d = 2$. The dashed line marks the HF transition temperature prediction ($T_\mathrm{c} \propto \exp(-a/|U|)$), and the square symbols are QMC data: The open square gives a scaled T_{KT}-value for $|U|/t = 4$ according to the work of Moreo *et al.*, the filled square shows our QMC result for $|U|/t = 4$, computed from the s-wave correlation function of one finite lattice (see also Fig. 3).

a phase diagram for the attractive Hubbard model in the temperature-interaction hyperplane qualitatively and quantitatively very close to the previously shown QMC data.

We included in these figure a QMC estimate for intermediate coupling calculated for a particular system size (compare Fig.3) and from an in-depth KT-scaling analysis after Moreo *et al.* [25]. For comparison the HF data are included, too. We see that the important qualitative feature is properly described: the critical temperature vanishes in both limits, $U \to 0$ and $U \to \infty$, with a maximum in between. In the weak coupling limit the line approaches asymptotically the HF data, whereas in the strong coupling regime a t^2/U dependence is approached, as expected in the Sections 3.2 and 3.3. Noting that in the Hartree-Fock treatment, leading to T_c^HF, phase fluctuations are entirely neglected, it is clear that the reduction of the transition temperature from T_c^HF must be attributed to these fluctuations. The large deviations for $|U|/t > 2$ clearly reveal that these fluctuations must be included to obtain a valid description of the physics. It should be kept in mind, however, that the expression (3.5) for the helicity modulus does not include the topological excitations (vortex-antivortex pairs) that the Kosterlitz-Thouless theory considers. The fact that the HF-expression for Υ_s is unrenormalized implies that the estimates are upper bounds, as implicitly suggested by the properly scaled QMC datum in Figure 15. Nevertheless, because the helicity modulus measures the free energy increment associated with twisting the direction of the order parameter, it becomes clear

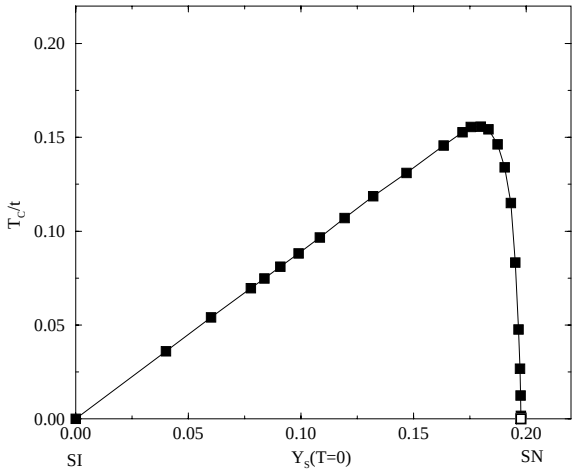

Fig. 16. "Uemura-Plot": T_c *versus* Y_s, const. $\rho = 0.4$, variation of the control parameter $\delta = 1/U$. This graph allows us to plot the dependence of two experimentally accessible quantities, the critical temperature and the superfluid condensate density $\rho_s \propto \Upsilon_s(T = 0)$ without an explicitly dependence on the particular 'control parameter' δ. 'SI' denotes the superconductor to insulator critical endpoint, 'SN' the superconductor to normal metal point.

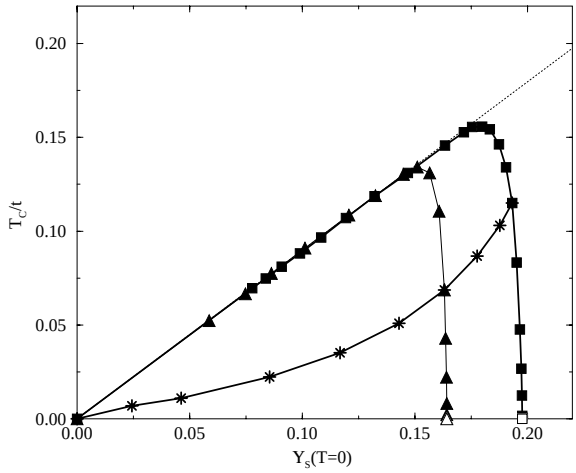

Fig. 17. "Uemura-Plot", similar to Figure 15: variation of U, constant filling $\rho = 0.4$ (square symbols), $\rho = 0.25$ (triangles) and variation of ρ, constant $U/t = -2.0$ (weak coupling regime, stars). Whereas in the strong coupling regime the data points collapse onto a single universal line, $T_c = 0.898\Upsilon_s(T = 0)$, independent of the filling, the weak coupling regime is nonuniversal.

that the reduction of the transition temperature from the HF-values must be attributed to phase fluctuations, which in the approximation leading to Figure 15 does not include topological excitations. T_c^{HF} provides an estimate, below which uncondensed pairs occur within this approximative framework, nicely supported by the previous QMC phase diagram, Figure 3. There we estimated the pair formation temperature T^*, which we argued to be closely related to the HF data. The "true" transition temperature is reduced by phase fluctuations, which also suppress the occurrence of phase coherence (*i.e.* off-diagonal long-range order, superfluidity, superconductivity) in the intermediate temperature regime $T^* \leq T \leq T_c$. Below T_c the phase coherence is established and superconductivity occurs. It should be noted, however, that T^* (or rather T_c^{HF}) is by no means a rigourous borderline. Indeed, fluctuating pair correlations are present at all temperatures. Their strength decreases with rising temperature and does not necessarily vanish above T^*.

The emerging scenario for the 2D attractive Hubbard model phase diagram is sketched in Figure 16 in an Uemura-like "universality plot" [30] T_c *vs.* $\Upsilon_s(T = 0)$, *i.e.* critical temperature *versus* helicity modulus or rather superfluid density. This type of plot allows us to get rid of the specific control parameter driving the particular crossover ($|U|$ in case of the Hubbard model).

Again we can distinguish two distinct regions: The weak coupling limit close to the normal state—superconductor transition (SN), where the helicity modulus or rather the superfluid density approaches a finite value for $|U|/t \to 0+$ and the strong coupling limit $|U|/t \to \infty$, where the system finally undergoes a superconductor to insulator transition (SI). Clearly, in the strong coupling regime all data collapse onto a single universal curve $T_c = 0.898\Upsilon_s$, as predicted in the previous Sections 3.2 and 3.3. Therefore the strong coupling limit close to the SI transition occurring at $U \to \infty$ is universal, but in contrast for finite densities the weak coupling regime is nonuniversal. In particular, the weak coupling part of the curve is strongly ρ dependent, as one can see in Figure 17. The weak coupling curve approaches the universal curve and thus the SI critical endpoint asymptotically for $\rho \to 0$.

Whereas for different electron densities ρ (shown are $\rho = 0.25$ (squares) and $\rho = 0.4$ (triangles) curves) the *strong* coupling data collapse onto the *same* universal curve, the weak coupling parts are different, *i.e.* nonuniversal for finite ρ. The weak-coupling superfluid density is dominated by the concentration of available charge carriers ρ, as we can see in Figure 17: The stars show T_c *vs.* $\Upsilon_s(T = 0)$ for constant $|U|/t = 2.0$ and a series of electron densities $\rho = 0.025, 0.05, 0.1, \ldots, 0.4$. Vanishing ρ causes a non-universal curve; for the above mentioned trivial case $\rho \to 0$ the curve tends also to the SI fixpoint ('trivial' insulator transition in case of vanishing carrier concentration). Therefore, the weak coupling regime itself is characterized by a nonuniversal behavior; the universal line will only be re-approached when the system comes close to a further superconductor-insulator critical point in case of $\rho \to 0$, the "empty band insulator". The "Uemura-relation" becomes again linear und joins the strong coupling universal line.

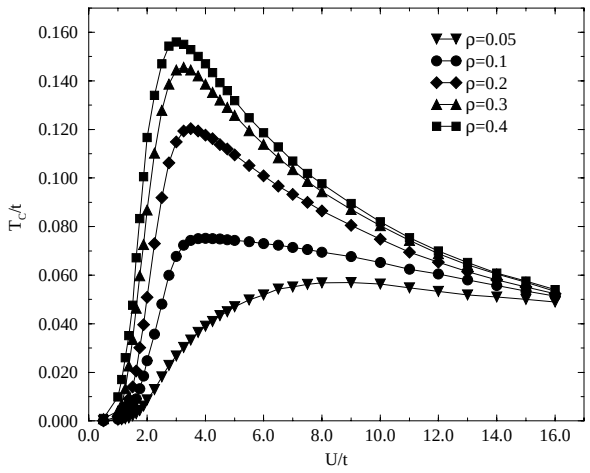

Fig. 18. $T_c(U)$ for various ρ-values; the maximum T_c^{max} as an estimate separating the meanfield and strong coupling regions shifts to higher U-values with decreasing ρ.

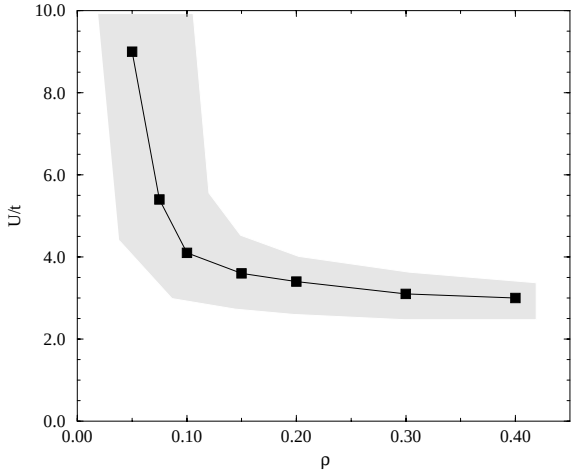

Fig. 19. $U(\rho)$: the data points depict the U-value, where a maximum in the appropriate $T_c(U)$-curve for fixed ρ appears; it serves appropriate $T_c(U)$-curve for fixed ρ appears; it serves as a measure to distinguish phase diagram regions where either a BCS (below the curve) or a strong coupling treatment (above the curve). The 'crossover' region along the U-axis is certainly not a singular point, but rather an extended transitional region, indicated by the grey shaded region.

Finally, we want to get a qualitative and approximately quantitative phase diagram for the attractive Hubbard model in the ρ-U-plane. For this purpose we extend the described approximation technique for the $T_c(U)$-line into the ρ-direction between $\rho \in [0; 0.5[$, Figure 18. As already stated earlier, there are two distinct regimes, the weak coupling one with critical exponent $z = 1$ and $T_c \propto \exp(-a/U)$ and the strong coupling regime with $z = 2$ and $T_c \propto 1/U$. To 'pin down' the crossover we use the position of the maximum T_c^{max}, which roughly distinguishes both regimes. Nevertheless, the 'crossover' regime is certainly not a sharp line, but rather a broad region, separating two extremal endpoints.

Figure 19 tries to depict this crossover line. It is worth noticing that the weak coupling regime shrinks to a rather small region for $\rho \to 0.5$ and extends up to the whole U-axis for $\rho \to 0$. This is in nice agreement with the naive estimate that a mean field approach should be valid in the whole interaction regime if $\rho \to 0+$.

5 Summary and conclusions

We provide a description of the phase diagram of the attractive Hubbard model in two dimensions, using numerical QMC data for finite lattices, as well as estimates from a Hartree-Fock approach for an onsite coupled lattice superconductor and from a corrected approach taking phase fluctuations into account. The phase diagram is characterized by the following distinct features:

- The weak coupling regime is rather well described by a mean field approach like HF; for $T = 0$, ρ fixed, the system undergoes a normal metal $U = 0$ to superconductor transition (NS, $|U| > 0$) as a function of coupling strength.
- For large coupling the HF estimates for the transition temperature increase, whereas a corrected approach, described in the present work and based on earlier publications of Denteneer *et al.* [15], finds a suppression of the transition temperature, which finally leads to $T_c \to 0$ for $|U| \to \infty$. This result nicely agrees with our QMC data. For $|U| \to \infty$ the system undergoes at $T = 0$ a superconductor-to-insulator transition (SI).
- At finite temperature in the weak coupling regime the mean-field description of the NS-transition applies, while in the large-U regime phase fluctuations dominate, accompanied by an increase of the critical regime.
- In the large U regime, where T_c^{HF} diverges, we find a regime where a pseudogap appears above T_c. We associate this pseudogap with the appearance of preformed pairs, which are formed at a temperature scale T^* far above the superconducting condensation temperature T_c. T_c^{HF} appears to be a rather good estimate for T^*, the 'true' condensation temperature is reduced to T_c by phase fluctuations, which suppress the occurence of phase coherence in the region between T^* and T_c. It should be noted, however, that T^* is by no means a rigorous borderline. Indeed, pairing correlations are present at all temperatures.
- An investigation of the band structure as a function of temperature (Fig. 5) reveals three qualitatively different regimes: (a) $T > T^*$: Only one band, roughly resembling the free band shape, exists. (b) $T^* > T > T_c$: Two bands, appearance of a pseudogap above T_c, no phase coherence. (c) $T_c \leq T$: 'BCS'-like band structure; the 'shape' of the band structure changes at the phase transition into a phase coherent superconducting

Table 1.

		z	$\bar{\nu}$	$\bar{\alpha}$
NS, normal metal to superconductor, interaction driven	ρ finite, $U \to 0+$	1	1/2	0
SI, superconductor to insulator, interaction driven	ρ finite, $U \to \infty$	2	1/2	0
NI, normal metal to insulator	$\rho \to 0$, $U = 0$	2	1/2	0
SIw, superconductor to insulator, weak coupling treatment, density driven	$\rho \to 0$, 'weak' U	1	1/2	0
SIs, superconductor to insulator, strong coupling treatment, density driven	$\rho \to 0$, 'strong' U	2	1/2	0
Non-interacting fermions, density driven MI transition	$\rho \propto (\mu - \mu_{\rm B})$			
Interacting fermions, QMC, finite density, weak coupling	$\rho \propto (\mu - \mu_{\rm B})^{1/2}$			
Interacting fermions, QMC, finite density, strong coupling	$\rho \propto (\mu - \mu_{\rm B})$			

state, but not the magnitude of the gap. We find extended 'flat' band regions above and below the Fermi edge ($\omega = 0$), similar to the appearance of a 'coherent particle peak' in ARPES experiments on underdoped cuprates at the transition from the pseudogap to the phase coherent regime [26,27]. Thus, the superconducting transition is clearly detectable in the shape of the band structure and the density of states.

– An Uemura-like plot of the critical temperature *versus* the helicity modulus or rather the superfluid density reveals, that the system shows an universal behavior in the strong coupling regime close to the SI transition, whereas the weak coupling regime is nonuniversal.
– We summarize the results for the critical exponents in Table 1, describing the phase diagram of the $D = 2$ attractive Hubbard model.
There are distinct transitions: The superconductor to normal state (NS) and superconductor to insulator (SI) for fixed ρ, occurring in the limits $U \to 0$ and $U \to \infty$, respectively, as well as density driven insulator transitions in the different U regimes. In this view the crossover from weak to strong coupling, or in other words, the crossover from BCS- to Bose-Einstein superconductivity corresponds to a crossover from a NS to a SI critical point, as revealed by the different exponents.

We thank H. Beck, R. Fresard and P. F. Meier for useful discussions, and H.-G. Matuttis for the collaboration on the quantum Monte-Carlo algorithms. The work was supported by the Swiss National Foundation for Science.

References

1. T. Schneider, J.M. Singer, Proc. Adriatico Res. Conf. "Fluctuation Phenomena in High Temperature Superconductors", edited by A. Ausloos *et al.* (Kluwer Academic, 1996).
2. T. Schneider, Proc. Europhys. Conf. "Physics of Magnetism 96", edited by R. Micnas, Acta Physica Polonica A (1996).
3. T. Schneider, J.M. Singer, unpublished (1997).
4. J.M. Singer, P.F. Meier, Research Report University of Zurich (1996); Proceedings of the 5th interntl. M^2S-HTSC-V Conference, Beijing, China 1997, to appear in Physica C (1997).
5. H. Ding, T. Yokoya, J.C. Campuzano, T. Takahashi, M. Randeria, M.R. Norman, T. Mochiku, K. Kadowaki, J. Giapintzakis, Nature **382**, 51 (4 July 1996).
6. A.G. Loeser, Z.-X. Shen, D.S. Dessau, D.S. Marshall, C.H. Park, P. Fournier, A. Kapitulnik, Science **273**, 325 (19 July 1996).
7. B. Batlogg, V.J. Emery, Nature **382**, 20 (4 July 1996).
8. M. Randeria, in *Bose-Einstein-Condensation*, edited by A. Griffin *et al.* (Cambridge University Press, Cambridge, England, 1994); M. Randeria, Proc. Adriatico Res. Conf. "Fluctuation Phenomena in High Temperature Superconductors", edited by A. Ausloos *et al.* (Kluwer Academic, 1996).
9. Y. Ando *et al.*, Phys. Rev. Lett. **77**, 2065 (1996); Phys. Rev. Lett. **77**, 5417 (1996).
10. T. Schneider, H. Keller, Int. J. Mod. Phys. B **5**, 487 (1993).
11. J.M. Singer, M.H. Pedersen, T. Schneider, H. Beck, H.-G. Matuttis, Phys. Rev. B **54**, 1286 (1996).
12. W. von der Linden, Phys. Rep. **220**, 53 (1992).
13. J. Gubernatis, M. Jarrell, R.N. Silver, D.S. Sivia, Phys. Rev. B **44**, 6011 (1991). M. Jarrell, J.E. Gubernatis, Phys. Rep. **269(3)**, 133 (1996).
14. J.E. Hirsch, Phys. Rev. B **31**, 4403 (1985); H.-G. Matuttis, PhD. Thesis, University of Regensburg, (1995).
15. P.J.H. Denteneer, Guozhong An, J.M.J. van Leeuwen, Phys. Rev. B **47**, 6256 (1993); P.J.H. Denteneer, Guozhong An, J.M.J. van Leeuwen, Europhys. Lett. **16**, 5 (1991).
16. Zhu-Pei Shi, R.R.P. Singh, Europhys. Lett. **31**, 219 (1995).
17. K. Michielsen, H. de Raedt, unpublished; J.M. Singer, unpublished.
18. K. Kim, P. Weichman, Phys. Rev. B **43**, 13583 (1991).
19. M.P.A. Fisher, P.B. Weichman, G. Grinstein, D.S. Fisher, Phys. Rev. B **40**, 546 (1989).
20. M.E. Fisher, M.N. Barber, D. Jasnov, Phys. Rev. A **9**, 1111 (1973).
21. A.L. Fetter, J.D. Walecka, *Quantum Theory of Many Particle Systems* (McGraw Hill, New York 1971).
22. M. Drechsler, M. Zwerger, Ann. Phys. **1**, 15 (1992).
23. R. Gupta *et al.*, Phys. Rev. Lett. **61**, 1996 (1988).
24. W. Janke, Phys. Lett. A **148**, 306 (1990).
25. A. Moreo, D.J. Scalapino, Phys. Rev. Lett. **66**, 946 (1991).
26. Z.-X. Shen, private communication, Aspen Winter Conference on Strongly Correlated Systems (1997).
27. J.-M. Imer, F. Patthey, B. Dardel, W.-D. Schneider, Y. Baer, Y. Petroff, Z. Zettl, Phys. Rev. Lett. **62**, 336 (1989).
28. J.M. Singer, M.H. Pedersen, T. Schneider, Physica B **230-232**, 995 (1997).
29. N. Furukawa, M. Imada, J. Phys. Soc. Jpn **61**, 3331 (1992).
30. Y. Uemura *et al.*, Phys. Rev. Lett. **62**, 2317 (1989); Phys. Rev. B **38**, 909 (1988).